High Temperatures-High Pressures, Vol. 52, pp. 229–247
Reprints available directly from the publisher
Photocopying permitted by license only
DOI: 10.32908/hthp.v52.1431

Dual-wavelength reflectance-ratio method for emissivity-free temperature measurements applied to electromagnetically levitated liquid Ni

HIDEKAZU KOBATAKE[1]*, MASAYA IWABUCHI[2], YUMA KUROKAWA[2], MAKOTO OHTSUKA[2], MASAYOSHI ADACHI[2], HIROYUKI FUKUYAMA[2], NAOHIKO SASAJIMA[3] AND YOSHIRO YAMADA[3,4]

[1]*Organization for Research Initiatives and Development Doshisha University, Japan*
[2]*Institute of Multidisciplinary Research for Advanced Materials, Tohoku University, Japan*
[3]*National Institute of Advanced Industrial Science and Technology, Tsukuba, Japan*
[4]*Current affiliation: National Physical Laboratory, Teddington, UK*

Received: January 24, 2023; Accepted: April 24, 2023.

The applicability of the dual-wavelength reflectance-ratio (DWR) method to emissivity-free radiation thermometry of electromagnetically levitated high-temperature liquid metals was investigated. To establish the measurement technique, the DWR method was applied to liquid Ni levitated in a static magnetic field, which suppresses the surface oscillation and the translational motion. In a previous study, temperature of the levitated liquid metals measured by DWR showed deviations of about 95 K to 175 K from the temperature measured by a calibrated pyrometer. Since this discrepancy could be attributed to the imperfect contribution of the auxiliary light, the effect of the optical setup of the auxiliary light on the temperature measurement was investigated in this study. By using a reflecting collimator for the auxiliary optical system and adopting the radiance ratio determined considering the geometrical arrangement of the measurement system, the difference between temperature of liquid Ni kept near its melting temperature ($T_m = 1728$ K) measured using DWR and the temperature measured by a pyrometer calibrated using the melting point of Ni was 12 K on average and the standard deviation in the temperature measurement was 25 K ($n = 5$).

Keywords: Temperature measurement, Electromagnetic levitation, Emissivity free, Dual-wavelength reflectance-ratio method, Auxiliary light, Liquid nickel

*Corresponding author: hkobatak@mail.doshisha.ac.jp

1 INTRODUCTION

Numerical simulation is becoming increasingly important in the liquid-phase processing of materials, such as casting [1], welding [2], additive manufacturing [3], and crystal growth [4]. Numerical simulation can be applied to understand manufacturing processes, predict casting defects, and optimize operating conditions, leading to cost reduction.

For accurate numerical simulations of processes, the thermophysical properties of materials, such as thermal conductivity, heat capacity, and surface tension, are required as input parameters [5]. However, despite the importance of thermophysical properties for numerical simulations, it has been difficult to measure these properties in the liquid phase owing to the high reactivity of the material under investigation, resulting in chemical contamination.

To solve this difficulty, the levitation technique has been developed to measure the thermophysical properties of metals and alloys in the liquid phase. Thermophysical properties, such as surface tension, have been measured using the oscillating droplet method [6–9], and the densities of liquid metals can be measured by obtaining a shadowgraph of the levitated droplet through which the volume is determined [10–12]. The viscosity can be measured from the damping relaxation time of the surface oscillation of the levitated droplet under electrostatic levitation [13] or microgravity [14–16]. A system for the measurement of high-temperature thermophysical properties, named PROSPECT, has been developed by the present authors. PROSPECT can be used to measure the heat capacity, thermal conductivity, and emissivity of liquid metals while suppressing translational motion, surface oscillation, and convection by applying a static magnetic field to levitate droplets electromagnetically using a superconducting magnet [17–24].

In these levitation systems, an optical pyrometer is normally used to measure the temperature. To use a single-color pyrometer for temperature measurements, the normal spectral emissivity of the sample must be known *a priori*. In most cases, however, the normal spectral emissivity of a high-temperature liquid in the measurement wavelength range of the pyrometer is unknown. Therefore, the emissivity of the liquid at a known temperature needs to be determined. At the melting temperature of a liquid sample, the sample emits light with radiance L_{m} at wavelength λ, which can be expressed in terms of the apparent melting temperature T_{ap} as follows:

$$L_{\mathrm{m}} = \frac{\varepsilon_{\mathrm{in}} hc^2}{\lambda^5 \{\exp(hc/k\lambda T_{\mathrm{ap}}) - 1\}}. \tag{1}$$

Here, h ($6.62607015 \times 10^{-34}$ J s) is the Planck constant, k (1.380649×10^{-23} J K^{-1}) is the Boltzmann constant, c (2.99792458×10^{8} m s^{-1}) denotes

the speed of light in a vacuum, and ε_{in} is the emissivity setting of the pyrometer. Because L_m corresponds to the radiance of the liquid metal at its melting temperature T_m, the true sample emissivity can be determined as ε_{cali} using the following relation:

$$\varepsilon_{cali} = \frac{L_m \lambda^5}{hc^2} \left\{ \exp\left(\frac{hc}{k\lambda T_m} \right) - 1 \right\}. \tag{2}$$

The temperature of the sample can be obtained using the determined emissivity with the assumption that the emissivity is constant with respect to temperature. However, there is no guarantee that the emissivity of the liquid metal is constant with temperature. In addition, emissivity data measured at approximately 680 nm by the pulse-heating technique with a fast ellipsometer show the possibility that the emissivity of some pure metallic liquids is dependent on the temperature [25].

Yamada et al. [26–29] have developed emissivity-free radiation thermometry using dual-polarization reflectance-ratio method for measuring silicon wafer surface temperature during rapid thermal processing [16, 28], and dual-wavelength reflectance-ratio (DWR) method for measuring temperature of rolled stainless-steel plate. In the former investigation, two spot radiometers detecting radiation with polarizations orthogonal to each other were utilized in combination with a planar heater comprising a Joule heated platinum foil as the auxiliary light source and a rapid chopper system. In the latter, a one-dimensional scanning-type photodiode detector was used to measure the radiance, and a SiC heater rod was applied as an auxiliary light source. Using these setups, they successfully measured the surface temperatures of silicon wafer [16, 28] and stainless-steel plate [28] during thermal processing.

The present authors have applied a high-brightness auxiliary light optical system to measure temperatures of curved surface of metals exposed to temperatures of 1000 K or higher [29, 30]. Previous research showed that the application of DWR enables measurements of the temperature of spherical metals within a standard uncertainty of 8 K to 1250 K [30].

For electromagnetically levitated liquid metals, however, the DWR method and the calibrated pyrometer provide temperatures that differ by approximately 95 K to 175 K [31]. This large inconsistency was thought to be caused by the insufficient radiance of the auxiliary light to detect the reflectance ratio of the sample, or to arise from aberrations of the auxiliary light due to the long distance between the sample, the detector, and the light source. To design optimal DWR optics for emissivity-free temperature measurements, we aimed to identify the influencing factors in the temperature measurement systems, which were used to propose a solution for accurate emissivity-free temperature measurements.

2 PRINCIPLE OF THE DUAL-WAVELEGTH REFLECTANCE-RATIO METHOD

The principle of DWR has already been explained in detail [28, 30]. Therefore, we provide a brief description of the measurement principle here. The measurement system for the DWR method consists of a dual-wavelength radiation thermometer and an auxiliary light source. The thermal radiances of a sample at temperature T measured at two wavelengths, λ_1 and λ_2, using a dual-wavelength radiation thermometer are denoted $L_{\lambda 1,\mathrm{off}}(T)$ and $\mathrm{L}_{\lambda 2,\mathrm{off}}(T)$, respectively. These radiances can be expressed using the blackbody radiances $L_{\mathrm{BB},\lambda 1}(T)$ and $L_{\mathrm{BB},\lambda 2}(T)$ at the same temperature and wavelengths as follows:

$$L_{\lambda 1,\mathrm{off}}(T) = \varepsilon_{\lambda 1} \cdot L_{\mathrm{BB},\lambda 1}(T) \tag{3}$$

$$L_{\lambda 2,\mathrm{off}}(T) = \varepsilon_{\lambda 2} \cdot L_{\mathrm{BB},\lambda 2}(T). \tag{4}$$

Here, $\varepsilon_{\lambda 1}$ and $\varepsilon_{\lambda 2}$ are the emissivity at wavelengths λ_1 and λ_2, respectively. When the auxiliary light source is turned on, the radiation from the sample surface, $L_{\lambda 1,\mathrm{on}}(T)$ and $L_{\lambda 2,\mathrm{on}}(T)$, increases as a result of the superimposition of the auxiliary light reflected from the sample surface and the thermal radiation of the sample as follows:

$$L_{\lambda 1,\mathrm{on}}(T) = \varepsilon_{\lambda 1} \cdot L_{\mathrm{BB},\lambda 1}(T) + \rho_{\lambda 1} \cdot L_{\lambda 1,\mathrm{LS}} \tag{5}$$

$$L_{\lambda 2,\mathrm{on}}(T) = \varepsilon_{\lambda 2} \cdot L_{\mathrm{BB},\lambda 2}(T) + \rho_{\lambda 2} \cdot L_{\lambda 2,\mathrm{LS}}, \tag{6}$$

where $\rho_{\lambda 1}$ and $\rho_{\lambda 2}$ indicate the reflectance of the sample and $L_{\lambda 1,\mathrm{LS}}$ and $L_{\lambda 2,\mathrm{LS}}$ are the radiances of the auxiliary light at wavelengths λ_1 and λ_2, respectively. Subtracting equation (3) from equation (5) gives reflectance $\rho_{\lambda 1}$ at λ_1 as follows:

$$\rho_{\lambda 1} = \frac{L_{\lambda 1,\mathrm{on}}(T) - L_{\lambda 1,\mathrm{off}}(T)}{L_{\lambda 1,\mathrm{LS}}}. \tag{7}$$

We can obtain the reflectance $\rho_{\lambda 2}$ at wavelength λ_2 from equations (4) and (6) in the same form as equation (7). The reflectance ratio of the sample, R_ρ, can be obtained from the reflectance at λ_1 and λ_2 as follows:

$$R_\rho = \frac{\rho_{\lambda 1}}{\rho_{\lambda 2}} = \frac{L_{\lambda 1,\mathrm{on}}(T) - L_{\lambda 1,\mathrm{off}}(T)}{L_{\lambda 2,\mathrm{on}}(T) - L_{\lambda 2,\mathrm{off}}(T)} \cdot \frac{L_{\lambda 2\mathrm{LS}}}{L_{\lambda 1,\mathrm{LS}}} = \frac{L_{\lambda 1,\mathrm{on}}(T) - L_{\lambda 1,\mathrm{off}}(T)}{L_{\lambda 2,\mathrm{on}}(T) - L_{\lambda 2,\mathrm{off}}(T)} \cdot \frac{1}{R_{\mathrm{LS}}}. \tag{8}$$

Here, R_{LS} is the radiance ratio of the auxiliary light source, which can be determined independently of the material properties of the sample. Therefore, the reflectance ratio R_ρ can be expressed as a function of four measurable radiances.

By applying Kirchhoff's law, ($\varepsilon + \rho = 1$), the reflectance at two different wavelengths is described by equations (3′) and (4′):

$$\rho_{\lambda 1} = \frac{L_{\mathrm{BB},\lambda 1}(T) - L_{\lambda 1,\mathrm{off}}}{L_{\mathrm{BB},\lambda 1}(T)}. \tag{3′}$$

$$\rho_{\lambda 2} = \frac{L_{\mathrm{BB},\lambda 2}(T) - L_{\lambda 2,\mathrm{off}}}{L_{\mathrm{BB},\lambda 2}(T)}. \tag{4′}$$

Thus, using equations (3′) and (4′), the reflectance ratio of the sample is described as

$$R_\rho = \frac{\rho_{\lambda 1}}{\rho_{\lambda 2}} = \frac{L_{\mathrm{BB},\lambda 1}(T) - L_{\lambda 1,\mathrm{off}}}{L_{\mathrm{BB},\lambda 2}(T) - L_{\lambda 2,\mathrm{off}}} \cdot \frac{L_{\mathrm{BB},\lambda 2}(T)}{L_{\mathrm{BB},\lambda 1}(T)}. \tag{9}$$

From equation (9), the blackbody radiances at the sample temperature are describable with the following equations:

$$L_{\mathrm{BB},\lambda 1}(T) = \frac{L_{\lambda 1,\mathrm{off}} - \alpha(T) R_\rho \cdot L_{\lambda 2,\mathrm{off}}(T)}{1 - R_\rho} \tag{10}$$

$$L_{\mathrm{BB},\lambda 2}(T) = \frac{1\!\!\diagup\!\!\alpha(T) \cdot L_{\lambda 1,\mathrm{off}} - \alpha(T) R_\rho \cdot L_{\lambda 2,\mathrm{off}}(T)}{1 - R_\rho}. \tag{11}$$

Term $\alpha(T)\left(\equiv \dfrac{L_{\mathrm{BB},\lambda 1}(T)}{L_{\mathrm{BB},\lambda 2}(T)}\right)$ is the ratio of the radiance at two wavelengths of a blackbody at temperature T. The value of R_ρ can be determined using equation (8), and the blackbody radiance at the sample temperature can be determined from equations (10) and (11) with the numerical solution of iterative calculations. Therefore, the sample temperature without knowledge of the sample emissivity can be determined using Planck's law.

3 EXPERIMENTAL PROCEDURE

3.1 Experimental setup

To evaluate the DWR method for liquid metal samples, we used the thermophysical properties measurement system, PROSPECT. This system enables electromagnetic levitation with a static magnetic field. With the application of a static magnetic field, translational motion and surface oscillation can be

suppressed [8, 18–24]. Figure 1 shows a schematic illustration of the experimental setup. Metallic samples were electromagnetically levitated in a superconducting magnet with a controlled ambient gas. The sample temperature was measured with a single-color pyrometer (IMPAC, IGA-140, wavelength: 1600 nm) from the bottom and adjusted by blowing He gas with a controlled flow rate.

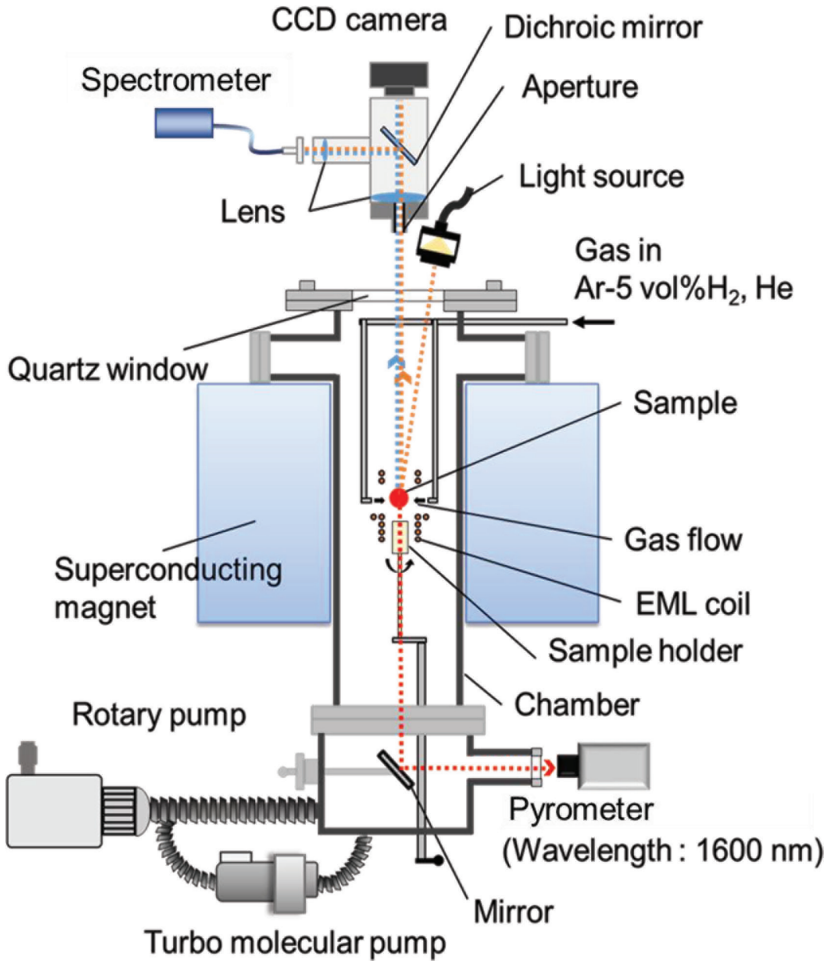

FIGURE 1
Schematic illustration of the experimental setup for temperature measurements using the dual-wavelength reflectance-ratio method. The liquid metal sample was electromagnetically levitated at the center of the chamber using a radio-frequency (rf) coil. A dc magnetic field was applied to prevent translational motion and surface oscillation of the liquid metal. The temperature at the bottom of the sample was monitored using a single-color pyrometer and controlled.

A spectroscope (Ocean Optics Inc., NIR Miniature Fiber Optic Spectrometer USB2000) was attached to an optical unit installed on top of the system to detect the sample radiance. Radiated light from the sample surface was focused on a spot of the glass fiber attached to the spectrometer using a lens equipped with an optical unit. The diameter of the focused area at the sample position was 4 mm. The wavelength detected using this device was between 780 nm and 1000 nm. The temperature was determined based on the DWR method by selecting two wavelengths as described in the results.

3.2 Calibration of the spectrometer

The spectrometer was calibrated using a standard light source, namely a quasi-blackbody made of graphite (Fig. 2). The blackbody cavity was 5 mm in diameter and 50 mm in depth. The whole cavity of the quasi-blackbody was surrounded by a metal bath to achieve a homogenized temperature distribution in the quasi-blackbody. To calibrate the spectrometer, the blackbody was placed at the same position as the levitated metal in the system and then uniformly heated by high-frequency induction heating. A single-color pyrometer was used for temperature measurements. The spectrometer was calibrated using the plateau temperatures detected during the melting and solidification of the metal in the surrounding metal bath. Details of the setup are provided in previously reported studies [18, 19]. The melting temperature, T_m, of Cu ($T_m = 1358$ K) and the eutectic temperature, T_E, of the Ni-C alloy ($T_E = 1602$ K) were used to calibrate the spectrometer.

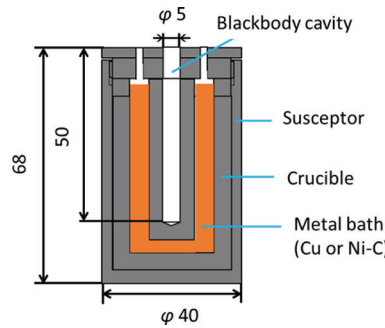

FIGURE 2
The quasi-blackbody used for spectrometer calibration. The quasi-blackbody hole was surrounded by a metal bath, which was used for temperature homogenization and as an internal reference, namely the melting temperature of Cu and eutectic temperature of binary Ni-C alloy.

3.3 Optical setup of the auxiliary light

The auxiliary light was supplied by a supercontinuum white light laser, which emits continuous light from 450 nm to 2500 nm through an optical fiber. This light source had a high radiance and high directivity. We used two different

types of optical systems: an aspherical lens (Fig. 3(a)) and a reflective collimator (Fig. 3(b)). The aspherical lens was used to avoid spherical aberration. Light from the optical fiber was focused onto the electromagnetically levitated sample surface. The reflective collimator was used to reduce the-effect of aberrations caused by differences in the refractive index of the lens at each wavelength.

Profiles of the radiance ratio at the light spot focused by the aspherical lens and reflective collimator were investigated prior to the temperature measurement using the DWR method. To measure the radiance profile of the auxiliary light, the spectrometer and the light source were coaxially arranged at 600 mm, as shown in Fig. 4(a). An aperture with a diameter of 1 mm was placed in front of the spectrometer. The radiance at the auxiliary light spot was scanned at an interval of 1 mm along the direction horizontal to the optical axis, and then the radiance ratio profile was obtained.

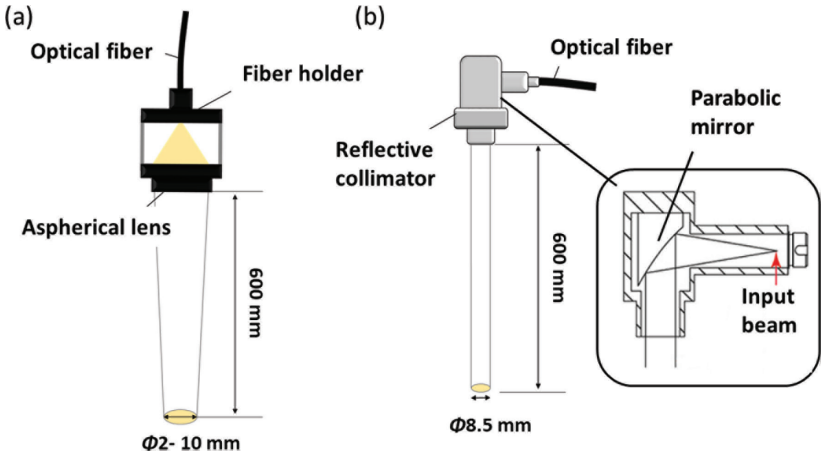

FIGURE 3
Schematic illustrations of the optical systems for the auxiliary light using a (a) aspherical lens, and (b) reflective collimator.

3.4 Evaluation of the radiance ratio of the auxiliary light

Prior to the measurement, the radiance ratio of the auxiliary light source was determined using a three-step procedure, as shown in Fig. 4. In the first step, the direct light ($R_{\mathrm{LS,\,Direct}}$) was measured using an optical setup with a linearly arranged detector and light source (Fig. 4 (a)). In this arrangement, the center of the light source was focused on the detector. In this step, it is difficult to account for the effect of the spread of light reflected off the sample droplet surface.

In the second step (Fig. 4 (b)), the reflected light was measured via a standard diffuse reflector placed at the same position (approximately 600 mm)

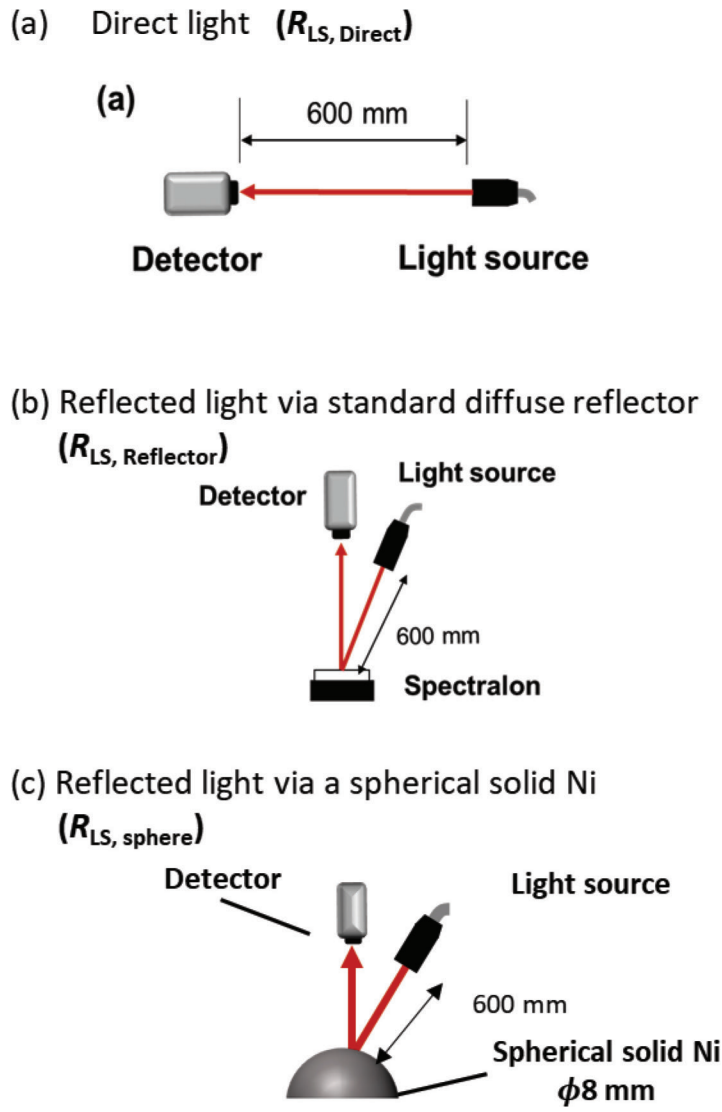

FIGURE 4
Schematic illustrations of the optical setup to evaluate the radiance ratio of the auxiliary light source, R_{LS}. (a) The direct light obtained with a linear arrangement of the detector and light source ($R_{LS, Direct}$). (b) The reflected light via the standard diffuse reflector placed at the same position as the electromagnetically levitated metallic liquid droplet considering the aberration of the auxiliary light passing the experimental optical path ($R_{LS, Reflector}$). (c) The reflected light via the solid Ni sphere ($R_{LS, Sphere}$) imitating the reflective properties of the electromagnetically levitated droplet.

from the detector as the electromagnetically levitated metallic liquid droplet ($R_{\mathrm{LS,\ Reflector}}$). In this step, the effect of the angle of the reflection and the aberration related to the distance of the detector from the light source should be considered.

In the last step, the reflected light was measured via an imitated spherical solid (Fig. 4 (c)). The radiance ratio of the auxiliary light reflected from spherical solid Ni ($R_{\mathrm{LS,Sphere}}$) was measured. By re-considering the geometry of the sample, we attempted to reproduce the reflective properties of the electromagnetically levitated droplet. In this study, we used a spherical solid Ni with a diameter of 8 mm to evaluate $R_{\mathrm{LS,Sphere}}$ assuming unity of the reflectance ratio.

4 RESULTS

4.1 Spatial distribution of the radiance ratio of the auxiliary light

Profiles of the count intensities, $X_{\mathrm{C}}(\lambda)$, across the auxiliary light spot focused by the aspherical lens and reflective collimator are shown in Fig. 5(a) and

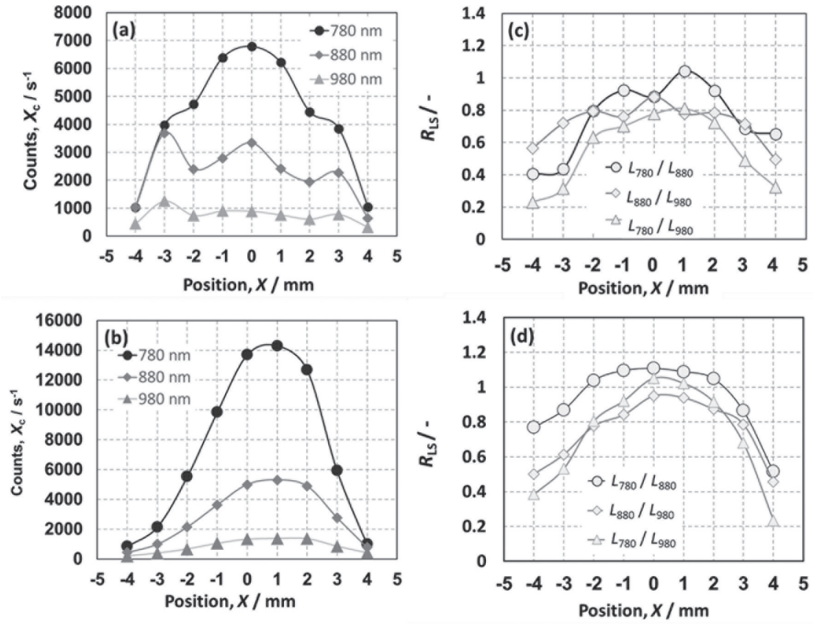

FIGURE 5
Profiles of the count intensities, $X_{\mathrm{C}}(\lambda)$, across the auxiliary light spot emitted through the (a) aspherical lens and (b) reflective collimator. The output count intensities of the light measured at the wavelengths of 780 nm (●), 880 nm (◆), and 980 nm (▲) are plotted in the figures. The radiance ratios, R_{LS}, namely L_{780} / L_{880} (○), L_{880} / L_{980} (◇), and L_{780} / L_{980} (△), for (c) the aspherical lens and (d) reflective collimator are plotted in the figures. The center of the auxiliary light spot corresponds to $X = 0$ mm.

5(b), respectively. The output count intensities of the light measured at the wavelengths of 780 nm (●), 880 nm (◆), and 980 nm (▲) were plotted. Each radiance ratio, R_{LS}, namely L_{780} / L_{880} (○), L_{880} / L_{980} (◇), and L_{780} / L_{980} (△), obtained with the aspherical lens and reflective collimator was also plotted in Fig. 5(c) and 5(d), respectively. The center of the auxiliary light spot corresponds to the coordinate of $X = 0$ mm.

By using the aspherical lens (Fig. 5(a)), profiles of the output count intensities of the light had inflection points at approximately $X = -3$ mm and 3 mm, indicating that the aberration caused by the lens remained. This aberration in the light-intensity profiles resulted in highly varied radiance ratios (R_{LS}), as shown in Fig. 5(c).

Figure 5(b) shows profiles of the output count intensities of the auxiliary light obtained with the reflective collimator. Unlike the profiles obtained with the aspheric lens, profiles of the count intensities at each wavelength obtained with the reflective collimator had a single smooth peak. Each radiance ratio (R_{LS}) of the auxiliary light obtained with the reflective collimator also showed a smooth profile, as shown in Fig. 5(d). In particular, the radiance ratios at the wavelengths of 780 nm and 880 nm showed a constant region from $X = -2$ mm to 2 mm. These results indicate that the radiance ratio at 780 nm and 880 nm of the auxiliary light source via a reflective collimator is optimal for temperature measurements using the DWR method.

4.2 DWR temperature measurement

Figure 6(a) shows an example of the spectral radiation of electromagnetically levitated liquid Ni at 1730 K, near the melting temperature of Ni (1728 K), at the wavelengths of 780 nm, 880 nm, and 980 nm. Figure 6(b) and 6(c) shows the top images of liquid Ni without and with auxiliary light illumination, respectively. When the auxiliary light was turned on for 60 s, the radiance at each wavelength increased due to the superimposition of the reflected auxiliary light. The spectral radiances at 880 nm and 780 nm were less disperse than that at 980 nm and thus were used to determine the temperature via DWR.

The temperature at the bottom of liquid Ni was measured using a single-color pyrometer, which was calibrated using the melting temperature of Ni. The temperature of liquid Ni was adjusted to approximately the melting temperature of Ni by controlling the He gas flow rate. Even if the emissivity of liquid Ni depends on the temperature, the difference between the real temperature and that measured using the single-color pyrometer is small at the melting temperature of Ni. Here, we defined the temperature measured using the single-color pyrometer as the reference temperature, T_{ref}.

The difference between the reference temperature (T_{ref}) and the temperature determined using DWR (T_{DWR}) is summarized in Table 1. The reference temperatures for the DWR temperature measurements using the aspherical lens and reflective collimator were 1730 K and 1728 K, respectively. T_{DWR} was calculated using three radiance ratios of the auxiliary light, which were

determined using the direct light ($R_{LS,\ Direct}$), reflected light via the standard diffuse reflector combination with the reflective collimator ($R_{LS,\ Reflector}$), and spherical solid Ni ($R_{LS,\ Sphere}$).

TABLE 1
Difference in the measured temperature using DWR and reference temperature. The wavelength used for the measurements were $\lambda_1 = 780$ nm and $\lambda_2 = 880$ nm

Radiance ratio of the auxiliary light	Aspherical lens (T_{ref} = 1730 K)		Reflective collimator (T_{ref} = 1728 K)	
	R_{LS}	$T_{ref} - T_{DWR}$	R_{LS}	$T_{ref} - T_{DWR}$
$R_{LS,\ Direct}$	0.95	n.a.	1.15	n.a.
$R_{LS,\ Reflector}$	1.25	86 K	1.23	n.a.
$R_{LS,\ Sphere}$	1.15	43 K	1.32	23 K

By using $R_{LS,\ Sphere}$, T_{DWR} measured with the aspherical lens and reflective collimator differed from the reference temperature by 43 K and 23 K, respectively. These deviations are much smaller than those of our previous report, which are from 95 K to 175 K [31]. Moreover, the numerical calculation diverged and gave no solution when $R_{LS,\ Direct}$ was used for both measurements. By using $R_{LS,\ Reflector}$, the numerical calculation gave no solution for the measurement with the reflective collimator. Although the numerical calculation using $R_{LS,\ Reflector}$ for the measurement with the aspherical lens gave a solution, the difference between the reference temperature T_{ref} and T_{DWR} was 86 K, which was much larger than those of determined by using $R_{LS,\ Sphere}$. The effect of the R_{LS} value on the temperature measurement will be discussed in Section 5.1.

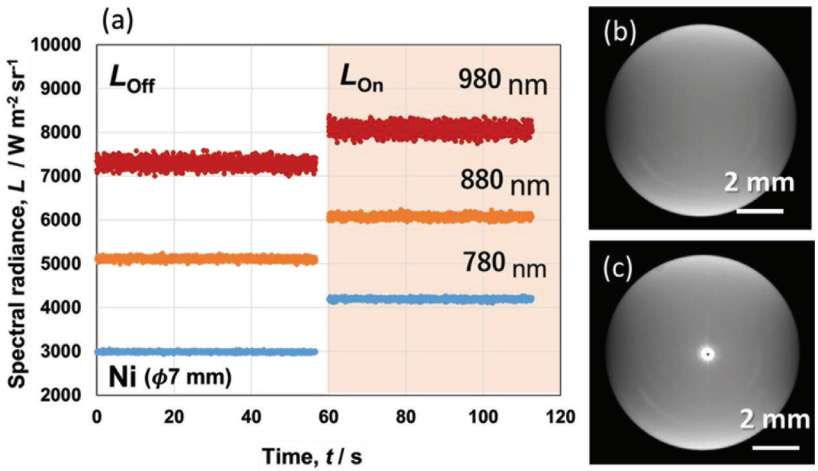

FIGURE 6
(a) Time-dependent radiance profile at the wavelengths of 780 nm, 880 nm, and 980 nm before and after auxiliary light illumination for liquid Ni at 1730 K. The aspherical lens was used to obtain the data. The top image of the levitated liquid sample (b) without auxiliary light illumination and (c) with the auxiliary light illumination are also shown.

4.3 Repeatability of the DWR method

The repeatability of the DWR temperature measurement was investigated for electromagnetically levitated liquid Ni kept at 1729 K by repeating auxiliary light illumination with the reflective collimator, as shown in Fig. 7. The auxiliary light was turned on for 5 s to obtain the superimposed radiance of the reflection, and then turned off for 5 s to obtain the radiation from the sample without light reflection. This operation was repeated five times to determine the temperature via DWR using each combination of the radiances with and without auxiliary light illumination, and the results are presented in Table 2. $R_{LS,\,Cal}$ calculated from T_{ref}, which will be discussed in the next section, is also listed. The radiances at the wavelengths of 780 nm and 880 nm were used to determine the temperature using the DWR method. The temperature of liquid Ni measured by the DWR method is on average 12 K lower than the reference temperature. In this investigation, the temperature measurements by DWR and the reference temperature measurements by the calibrated pyrometer were carried out on the upper and lower surfaces, respectively. Tsukada et al. [20] have investigated the temperature distribution in the electromagnetically levitated liquid silicon in a static magnetic field by numerical simulation. According to their investigation, the top surface temperature is approximately 10 K lower than that of the bottom surface of the levitated liquid Si in the static magnetic field of 4T due to the heterogenous heating induced by electromagnetic levitation on the ground. Therefore, one of the causes of this

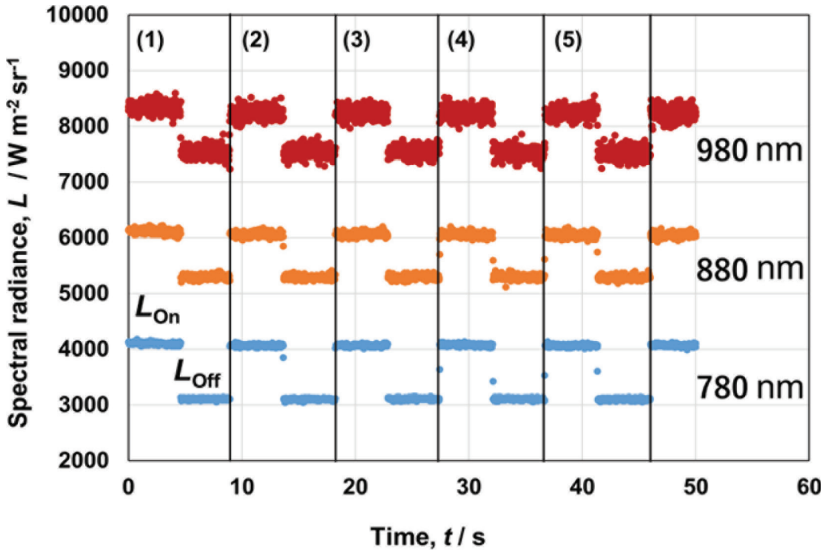

FIGURE 7
Radiance profile at the wavelengths of 780 nm, 880 nm, and 980 nm with intermittent auxiliary light illumination at 1729 K. The duration of auxiliary light illumination and non-illumination was 5 s.

TABLE 2
Repeatability in the temperature measurement using DWR at $T_{ref} = 1729$ K. The wavelength used for the measurements were $\lambda_1 = 780$ nm and $\lambda_2 = 880$ nm

No.	$R_{LS,\,Cal}$	T_{DWR}	$T_{ref} - T_{DWR}$
(1)	1.25	1679	51
(2)	1.30	1716	13
(3)	1.29	1712	17
(4)	1.31	1732	−3
(5)	1.32	1745	−16
Average	1.29	1717	12
Standard deviation	0.03	25	25

systematic temperature difference could be attributed to the temperature difference between the top and bottom surfaces of the sample. The type A uncertainty in temperature measurement using the DWR was evaluated to be 25 K ($n = 5$), where n is the number of measurements, by taking the experimental standard deviation of the measured temperatures.

5 DISCUSSION

As described in Section 2, the sample temperature can be determined using equation (10) or (11), the radiances at two wavelengths with and without auxiliary light illumination, and the radiance ratio of the auxiliary light, R_{LS}. The temperature determined using the DWR method strongly depends on R_{LS}. In this section, the dependence of the DWR temperature measurement on R_{LS} is discussed.

The relation between the DWR temperature and R_{LS} can be obtained using four parameters of the radiances, namely $L_{\lambda 1,\,on}(T)$, $L_{\lambda 2,\,on}(T)$, $L_{\lambda 1,\,off}(T)$, and $L_{\lambda 2,\,off}(T)$, which can be determined experimentally and by rearranging equation (10) as follows:

$$R_{LS} = \frac{R_{\Delta L}(T)\cdot\{L_{BB,\lambda 1}(T) - \alpha(T)\cdot L_{\lambda 2,off}(T)\}}{L_{BB,\lambda 1}(T) - L_{\lambda 1,off}(T)}, \tag{12}$$

where $R_{\Delta L}(T)$ is

$$R_{\Delta L} = \frac{L_{\lambda 1,on}(T) - L_{\lambda 1,off}(T)}{L_{\lambda 2,on}(T) - L_{\lambda 2,off}(T)}. \tag{13}$$

The temperature is contained in terms $L_{BB,\lambda 1}(T)$ and $\alpha(T)$. Using this equation, the temperature via DWR can be plotted as a function of R_{LS}. The four parameters, $L_{780,\,on}(T)$, $L_{780,\,off}(T)$, $L_{880,\,on}(T)$, and $L_{880,\,off}(T)$, used to plot the relation were experimentally measured (Table 3). Figure 8 shows the relation between the temperature and R_{LS} (T–R_{LS} curve) for measurements using the aspherical lens (a) and reflective collimator (b). These figures show that T is highly dependent on R_{LS}. For small R_{LS}, the slope of the curve is steep, and T is strongly dependent on R_{LS}. For large R_{LS}, the slope of the curve becomes gentle, and T is weakly dependent on R_{LS}. This means that in DWR measurements, the uncertainty in the measured temperature is smaller when an auxiliary light source with a larger R_{LS} is used.

TABLE 3
Parameters used to calculate the T–R_{LS} curve. The reference temperature, T_{ref}, and calculated radiance ratio, $R_{LS,Cal}$, are also listed. The wavelength used for the measurements were 780 nm and 880 nm

Optical setup.	$L_{780,off}$ / W m^{-2} sr^{-1} µm^{-1}	$L_{780,on}$ / W m^{-2} sr^{-1} µm^{-1}	$L_{880,off}$ / W m^{-2} sr^{-1} µm^{-1}	$L_{880,on}$ / W m^{-2} sr^{-1} µm^{-1}	T_{ref} / K	$R_{LS,Cal}$
Aspherical lens	3091	3544	5306	5725	1730	1.11
Reflective collimator	2989	4192	5112	6075	1728	1.29

The R_{LS} values obtained using the direct light ($R_{LS,\,Direct}$), reflected light via the standard diffuse reflector ($R_{LS,\,Reflector}$), and reflected light via spherical solid Ni ($R_{LS,\,Sphere}$) are indicated in the figures. The intersection of the T–R_{LS} curve and R_{LS} gives T_{DWR}.

Conversely, when the temperature is known, we can obtain the R_{LS} value, denoted $R_{LS,\,Cal}$, satisfying $L_{780,\,on}(T)$, $L_{780,\,off}(T)$, $L_{880,\,on}(T)$, and $L_{880,\,off}(T)$ obtained with measurements conducted near the melting temperature of Ni. The values of $R_{LS,\,Cal}$ are presented in Fig. 8 (a) and 8(b) to give T_{ref} (1730 K and 1728 K). Good agreement was found between $R_{LS,\,Sphere}$ and $R_{LS,\,Cal}$ in both figures. The difference between T_{ref} and T_{DWR} was found to be minimal when R_{LS} was obtained using the reflective collimator and a spherical solid, as shown in Fig. 8 (b). Thus, because light aberration is reduced, the reflective collimator is better than the aspherical lens in the optical system for the auxiliary light source. However, both $R_{LS,\,Direct}$ and $R_{LS,\,Reflector}$ of the reflective collimator did not intersect with the curve. The accuracy of the temperature measurement using DWR was improved by considering the geometrical arrangement of the measurement system in the determination of R_{LS}.

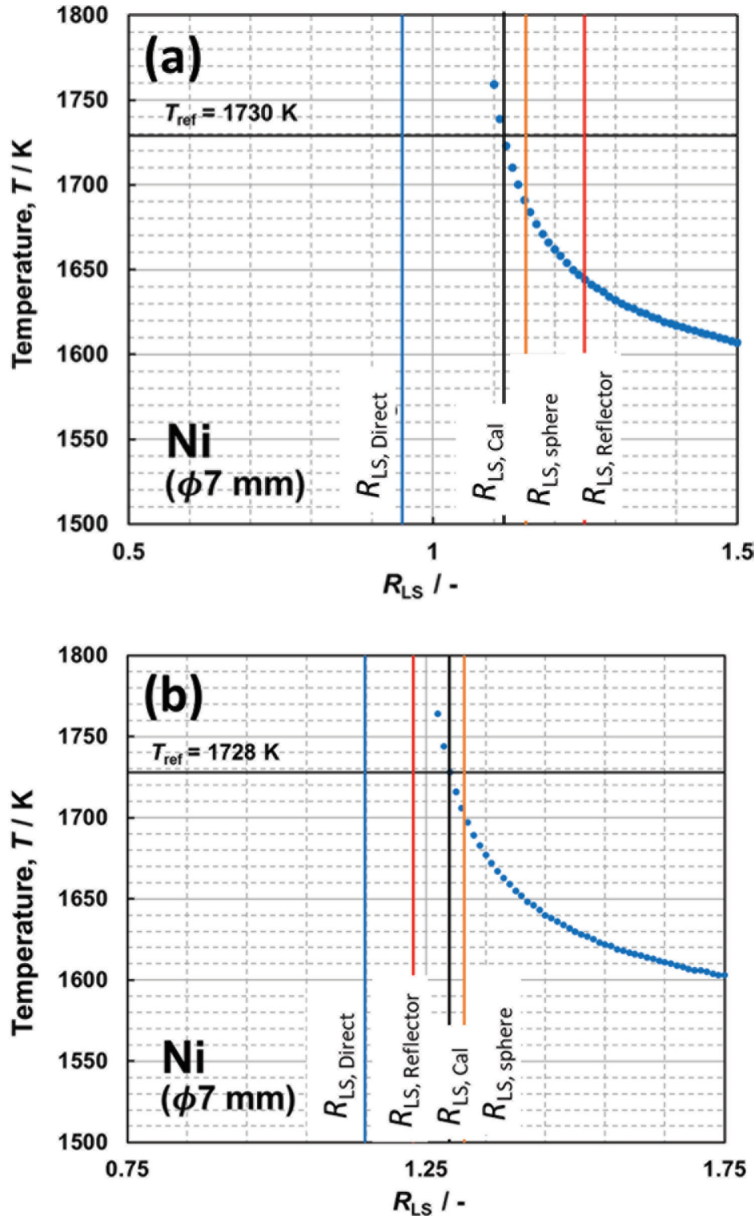

FIGURE 8
Relation between R_{LS} and temperature, calculated from equation (12) with the values of $L_{780,\,on}(T_m)$, $L_{880,\,on}(T_m)$, $L_{780,\,off}(T_m)$, and $L_{880,\,off}(T_m)$ measured using (a) the aspherical lens and (b) reflective collimator. The radiance ratio of the auxiliary light obtained from measurements of the direct light ($R_{LS,\,Direct}$), reflected light via the standard diffuse reflector ($R_{LS,\,Reflector}$), and reflected light via the spherical solid Ni ($R_{LS,\,Sphere}$) and calculated ($R_{LS,\,Cal}$) from the reference temperature (T_{ref}) are also indicated.

6 CONCLUSION

The effect of the auxiliary light source on the temperature measurement using the DWR method was experimentally investigated. The radiance ratio of the auxiliary light should be determined by considering the geometric arrangement of the measurement system. Use of a reflective collimator was a better auxiliary light source arrangement owing to the lack of optical aberration. By re- considering the geometrical arrangement of the measurement system, the accuracy of the temperature measurement was improved. The temperature of liquid Ni measured using the DWR differed from the reference temperature measured using a pyrometer calibrated in a conventional manner by 12 K on average, and the standard deviation in the measured temperature was 25 K ($n = 5$).

ACKNOWLEDGEMENT

This work was supported by JSPS KAKENHI Grant-in-Aid for Challenging Research (Pioneering) Grant Number JP16K14169 and Grant-in-Aid for Scientific Research (B) Grant Number 20H02490, as well as the JFE 21st Century Foundation and Matching Program between Tohoku University and AIST. We thank Edanz (https://jp.edanz.com/ac) for editing the draft of this manuscript.

REFERENCES

[1] M. Jolly, L. Katgerman, *Modelling of defects in aluminium cast products*, Progress in Materials Science **123** (2022) 100824, https://doi.org/10.1016/j.pmatsci.2021.100824

[2] D. P. Lukanin, V. V. Kalaev, Y. N. Makarov, T. Wetzel, J. Virbulis, W. Ammon, *Advances in the simulation of heat transfer and prediction of the melt-crystal interface shape in silicon CZ growth* J. Cryst. Growth **266** (2004) 20–27, https://doi.org/10.1016/j.jcrysgro.2004.02.025

[3] R-G. Vázquez, M. Holger, H-M. Koch, A. Otto A, *Multi-Physical Simulation of Laser Welding*, Phys. Proc. **56** (2014) 1334–1342, https://doi.org/10.1016/j.phpro.2014.08.059

[4] F-J. Gürtler, M. Karg, K-H. Leitz, M. Schmidt, *Simulation of laser beam melting of steel powders using the three-dimensional volume of fluid method,* Phys. Proc. **41** (2013) 881–886, https://doi.org/10.1016/j.phpro.2013.03.162

[5] T. Hibiya, I Egry, *Thermophysical property measurements of high temperature melts: results from the development and utilization of space*, Meas. Sci. Technol. **16** (2005) 317–326, https://doi.org/10.1088/0957-0233/16/2/001

[6] L. Rayleigh, *On the Capillary Phenomena of Jets*, Proc. R. Soc. Lond. (1879) 71–97, https://doi.org/10.1098/rspl.1879.0015

[7] I. Egry, H. Giffard, S. Schneider, *The oscillating drop technique revisited*, Mater. Sci. Technol. **16** (2005) 426–431, https://doi.org/10.1088/0957-0233/16/2/013

[8] S Ozawa, N Takenaga, T Koda, T Hibiya, Hidekazu Kobatake, Hiroyuki Fukuyama, Masayoshi Adachi, M Watanabe, Satoshi Awaj, *Oscillation behavior of a high-temperature silicon droplet by the electromagnetic levitation technique superimposed with a static magnetic field*, Materials Science and Engineering: A **495** (2008) 50–53, https://doi.org/10.1016/j.msea.2007.07.103

[9] H. Kobatake, J. Brillo, J/ Schmitz, P. Y. Pichon Surface tension of binary Al-Si liquid alloys, J Mat. Sci., **50** (2015) 3351–3360, https://doi.org/10.1007/s10853-015-8883-6
[10] J. Brillo, I. Egry, I. Ho, Density and Thermal Expansion of Liquid Ag–Cu and Ag–Au Alloy, Int. J. Thom., **26** (2006) 494–506, https://doi.org/10.1007/s10765-005-0011-4
[11] H. Kobatake, J. Brillo, Density and thermal expansion of Cr-Fe, Fe-Ni, and Cr-Ni binary liquid alloys, J. Mat. Sci., **48** (2013) 4934–4941, https://doi.org/10.1007/s10853-013-7274-0
[12] H. Kobatake, J. Brillo, Density and viscosity of ternary Cr–Fe–Ni liquid alloys, J. Mat. Sci., **48** (2013) 6818–6824, https://doi.org/10.1007/s10853-013-7487-2
[13] T. Ishikawa, P. F. Paradis, J. T. Okada, Y. Watanabe, Viscosity measurements of molten refractory metals using an electrostatic levitator, Meas. Sci. Technol. **23**, 025305, https://doi.org/10.1088/0957-0233/23/2/025305
[14] H. Kobatake. J. Brillo, Surface tension and viscosity measurement of ternary Cr-Fe-Ni liquid alloys measured under microgravity during parabolic flights, High Temp. High Press. **47** (2018) 465–477.
[15] X, Xiao, J. Brillo, L. Jonghyun, R. W. Hyers, D. M. Matson, *Impact of convection on the damping of an oscillating droplet during viscosity measurement using the ISS-EML facility*, **36** (2021). https://doi.org/10.1038/s41526-021-00166-4
[16] G. Lohöfer. *Viscosity Measurement by the "Oscillating Drop Method": The Case of Strongly Damped Oscillations*, Int. J. Thermo. **41** (2020) 30, https://doi.org/10.1007/s10765-020-2608-z
[17] H. Fukuyama, H. Kobatake, K. Takahashi, I. Minato, T. Tsukada, S. Awaji, *Development of Modulated Laser Calorimetry using a Solid Platinum Sphere as a Reference*, Meas. Sci. Technol. **18** (2007) 2059–66, https://doi.org/10.1088/0957-0233/18/7/036
[18] H. Kobatake, H. Fukuyama, I. Minato, T. Tsukada, S Awaji, *Noncontact measurement of thermal conductivity of liquid silicon in a static magnetic field* Appl. Phys. Lett. **90** (2007) 094102, https://doi.org/10.1063/1.2710220
[19] H. Kobatake, H. Fukuyama, I. Minato, T. Tsukada, S. Awaji, *Noncontact modulated laser calorimetry of liquid silicon in a static magnetic field* J. Appl. Phys. **104** (2008) 054901, https://doi.org/10.1063/1.2966455
[20] T. Tsukada, K. Sugioka H, T. Tsutsumino, H. Fukuyama, H. Kobatake, *Effect of static magnetic field on a thermal conductivity measurement of a molten droplet using an electromagnetic levitation technique* Int. J. Heat Mass Trans. **52** (2009) 5152–57, https://doi.org/10.1016/j.ijheatmasstransfer.2009.04.020
[21] H. Fukuyama, K. Takahashi, S. Sakashita, H. Kobatake, T. Tsukada, S. Awaji, *Noncontact Modulated Laser Calorimetry for Liquid Austenitic Stainless Steel in dc Magnetic Field,* ISIJ International **49** (2009) 1436–1442, https://doi.org/10.2355/isijinternational.49.1436
[22] H. Kobatake, H. Fukuyama, T. Tsukada, S Awaji, *Noncontact modulated laser calorimetry in a dc Magnetic field for stable and supercooled liquid silicon*, Meas. Sci. Technol. **21** (2010), 025901, https://doi.org/10.1088/0957-0233/21/2/025901
[23] K. Sugie H. Kobatake, H. Fukuyama, Y. Baba, K. Sugioka, T. Tsukada, *Development of thermophysical property measurement for liquid Fe using noncontact laser modulation calorimetry* Tetsu-to-Hagane, **96** (2010) 673–82.
[24] K. Sugie, H. Kobatake, M. Uchikoshi, M. Isshiki, K. Sugioka, T. Tsukada, H. Fukuyama, *Noncontact Laser Modulation Calorimetry for High-Purity Liquid Iron*, J. J. Appl. Phys. **50** (2011) 11RD04, https://doi.org/10.1143/JJAP.50.11RD04
[25] G. Pottlacher, K. Boboridis, C. Cagran, T. Huepf, A. Seifter, B. Wilthan, *Normal spectral emissivity near 680 nm at melting and in the liquid phase for 18 metallic elements*, AIP Conference Proceedings **1552** (1) 704–709, https://doi.org/10.1063/1.4819628
[26] Y. Yamada, J. Ishii, *Emissivity Compensation Utilizing Radiance Distribution in Thermal Images for Temperature Measurement of Electronic Devices*, J. J. Appl. Phys. **50** (2011) 11RE04, https://doi.org/10.1143/JJAP.50.11RE04
[27] Y. Yamada, J Ishii, *Dual-Wavelength Reflectance-Ratio Method for Emissivity-Free Radiation Thermometry*, SICE Annual Conference 2014 September 9–12, Hokkaido University, Sapporo, Japan.
[28] Y. Yamada, J. Ishii, *Toward Reliable Industrial Radiation Thermometry*. Int J Therm. **36** (2015) 1699–1712, https://doi.org/10.1007/s10765-015-1870-y

[29] H. Kobatake, Y. Kurokawa, H. Fukuyama, N. Sasajima, Y. Yamaguchi, Y. Yamada, *Dual-wavelength reflectance-ratio (DWR) method applied to high-temperature metals*, Proc. 56th SICE Ann. Conf. (2017) 427–428.

[30] H. Kobatake, Y. Kurokawa, M. Iwabuchi, M. Adachi, M. Ohotsuka, H. Fukuyama, Y. Yamaguchi, Y. Yamada, N. Sasajima, Emissivity-free radiation thermometry for high-temperature metals using the dual-wavelength reflectance-ratio method, Meas. Sci. Technol. **34** (2023) 015010, https://doi.org/10.1088/1361-6501/ac8ca3

[31] M. Iwabuchi, Y. Kurokawa, H. Kobatake, M. Ohtsuka, H. Fukuyama, Y. Yamaguchi, N. Sasajima, Y. Yamada, *Application of Dual-Wavelength Reflectance-Ratio Method to Electromagnetic Levitated Liquid Metals*, 57 th Proc. SICE Ann. Conf. (2018) 1–3